

# Tuning the Emission Colour of Triphenylamine-Capped Cyclometallated Platinum(II) Complexes and Their Application in Luminescent Oxygen Sensing and Organic Light-Emitting Diodes

Wenting Wu,<sup>[a]</sup> Chuanhui Cheng,<sup>[b]</sup> Wanhua Wu,<sup>[a]</sup> Huimin Guo,<sup>[a]</sup> Shaomin Ji,<sup>[a]</sup> Peng Song,<sup>[c]</sup> Keli Han,<sup>[c]</sup> Jianzhang Zhao,<sup>\*[a]</sup> Xin Zhang,<sup>[a]</sup> Yubo Wu,<sup>[a]</sup> and Guotong Du<sup>[b,d]</sup>

**Keywords:** Phosphorescence / Luminescence / Sensors / Density functional calculations / OLEDs / Platinum

[(Aryl-ppy)Pt(acac)] (ppy = 2-phenylpyridine, acac = acetylacetonato) derivatives with triphenylamine (TPA) substituents on the ppy ligand have been prepared. The TPA fragment is either directly cyclometallated (**Pt-1**) or attached to the ppy ligand through a C–C single bond (**Pt-2**) or a novel  $\alpha$ -diketo group (**Pt-3**). All the complexes show room-temperature phosphorescence in fluid solution with emission bands in the range of 530–590 nm, which are red-shifted relative to the model complex [ppyPt(acac)] ( $\lambda_{\text{em}} = 486$  nm). This emission colour tuning effect is attributed to either an elevated HOMO energy caused by electron-donating TPA substitu-

ents on the ppy ligand or a decreased LUMO energy caused by the electron-trap effect of electron-withdrawing substituents; both result in a smaller HOMO–LUMO energy gap and thus red-shifted emission. The complexes show extended luminescence lifetimes ( $\tau = 3.0$ – $5.5$   $\mu\text{s}$ ) relative to the parent complex [ppyPt(acac)] ( $\tau = 2.6$   $\mu\text{s}$ ). The luminescent oxygen-sensing properties of the complexes were studied in solution and polymer films. White light emission was observed with an OLED device fabricated with complex **Pt-3** with CIE coordinates of (0.32, 0.32).

## Introduction

Cyclometallated Pt<sup>II</sup> or Ir<sup>III</sup> complexes are attractive triplet emitters and have been extensively studied as phosphorescent materials for electroluminescence (organic light-emitting diodes, OLEDs), molecular sensors and photo-responsive molecular devices.<sup>[1–19]</sup> The emissive excited states of these complexes are the mixed <sup>3</sup>MLCT/<sup>3</sup>IL state, thus the emissions are characterized by structured emission bands and large Stokes shifts.<sup>[3]</sup> Usually, cyclometallated Pt<sup>II</sup>/Ir<sup>III</sup> complexes with C<sup>^</sup>N ligands show high luminescent quantum yields and good photostability as well as long luminescent lifetimes in the range of microseconds ( $\mu\text{s}$ ).

Thus, these materials show promise for application as luminescent O<sub>2</sub>-sensing materials, which require long-lived triplet emitters.<sup>[20–39]</sup> However, to our surprise, no systematic study has been carried out on the application of these complexes as luminescent O<sub>2</sub>-sensing materials. Furthermore, we have noticed that OLEDs and luminescent O<sub>2</sub> sensing present the same challenge, that is, to tune the emission colour of the phosphorescent materials, for example, to achieve white light-emitting diodes or monochromatic emission in the blue, green and red regions. Furthermore, it is important to be able to vary the luminescent lifetimes of phosphorescent dyes for oxygen sensing and for use as OLEDs.<sup>[25]</sup>

Triplet emitters (phosphorescent dyes) with long luminescent lifetimes are used for luminescent O<sub>2</sub> sensing, for example, ruthenium polydiimine complexes such as [Ru(bpy)<sub>3</sub>]<sup>2+</sup> or platinum porphyrin complexes such as PtOEP.<sup>[20–25,32,33]</sup> Luminescent O<sub>2</sub> sensing is based on the quenching effect of O<sub>2</sub> on the phosphorescence emission of the complexes.<sup>[21,34–38]</sup> To address the drawbacks of emission-intensity-based O<sub>2</sub> sensing, lifetime-based sensing or ratiometric sensing is desired.<sup>[21–24]</sup> Lifetime-based O<sub>2</sub> sensing requires phosphorescent dyes with longer luminescent lifetimes.<sup>[25]</sup> In contrast, a short luminescent lifetime is preferred for OLED purposes to avoid saturation effects. However, it has been proven that the tuning of luminescent lifetimes of transition-metal complexes is elusive. To the best

[a] State Key Laboratory of Fine Chemicals, School of Chemical Engineering, Dalian University of Technology, 158 Zhongshan Road, Dalian 116012, P. R. China  
Fax: +86-411-3960-8007  
E-mail: zhaojzh@dut.edu.cn

[b] School of Physics and Optoelectronic Technology, Dalian University of Technology, Dalian 116024, P. R. China  
Fax: +86-411-8470-7865

[c] State Key Laboratory of Molecular Reaction Dynamics, Dalian Institute of Chemical Physics, Chinese Academy of Sciences, 457 Zhongshan Road, Dalian 116023, P. R. China

[d] State Key Laboratory of Integrated Optoelectronics, College of Electronic Science and Engineering, Jilin University, 2699 Qianjin Street, Changchun 130012, P. R. China

Supporting information for this article is available on the WWW under <http://dx.doi.org/10.1002/ejic.201000327>.

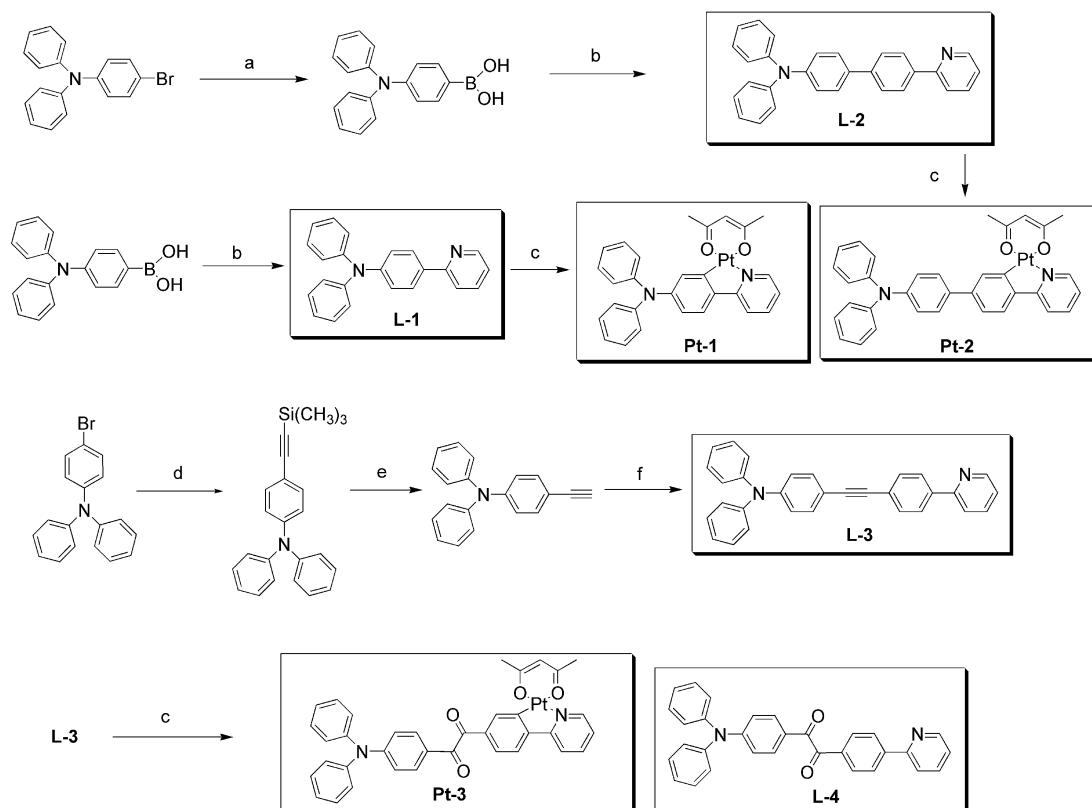
of our knowledge, very little effort has been made to tune the luminescent lifetimes of cyclometallated Pt complexes.

Herein we describe the synthesis of cyclometallated [Pt<sup>II</sup>(acac)] complexes with the triphenylamine (TPA)-integrated ppy ligand (**Pt-1**) (ppy = 2-phenylpyridine, acac = acetylacetonato)<sup>[4]</sup> or with the TPA fragment attached to the phenyl group of the ppy moiety either through a C–C single bond (**Pt-2**) or a novel  $\alpha$ -diketo moiety (**Pt-3**). The photophysics of the complexes were studied by UV/Vis absorption, luminescence emission spectra and theoretical calculations (DFT/TDDFT). The complexes show phosphorescence emission bands in the range of 490–561 nm. The red-shifted emission of the complexes relative to the parent complex [ppyPt(acac)] ( $\lambda_{\text{em}} = 486$  nm) is attributed to the increased HOMO energy or the decreased LUMO energy, as suggested by DFT calculations. The complexes were found to be sensitive luminescent oxygen-sensing materials. A white light-emitting OLED was fabricated with **Pt-3**. To the best of our knowledge no cyclometallated Pt<sup>II</sup> complexes have been systematically studied for luminescent O<sub>2</sub>-sensing purposes. The structure–emission relationship revealed by our study will be useful in the design of phosphorescent emissive materials.

## Results and Discussion

### Design and Synthesis of the Ligands and Cyclometallated Pt<sup>II</sup> Complexes

The design rationale of the Pt complexes lies in the notion that attaching an electron-donating group to the phenyl group of ppy will increase the energy of the HOMO, but the energy of the LUMO will be hardly affected; thus, the band gap ( $\Delta E_{\text{HOMO-LUMO}}$ ) of the complex will be reduced and red-shifted emission will be observed.<sup>[1,4]</sup> Different linkers, such as a C–C single bond and a  $\alpha$ -diketo moiety, were used to connect the triphenylamine (TPA) and the phenylpyridine (ppy) to investigate the effect of coupled and decoupled  $\pi$ -conjugated systems on the photophysical properties of the complexes. Pd-catalysed Suzuki and Sonogashira coupling reactions were used to prepare the ligands.<sup>[25]</sup> Metallation of the ligands with [K<sub>2</sub>PtCl<sub>4</sub>] and then reaction with Hacac led to the cyclometallated Pt complexes (Scheme 1). We found an unexpected  $\alpha$ -diketo product in the metallation with the ethynyl ligand (**Pt-3**). This is probably due to Pt-catalysed oxidation of the –C≡C– bonds.<sup>[40,41]</sup> All the intermediates and the final Pt complexes were obtained in satisfactory yields.



Scheme 1. Synthesis of the ligands and the cyclometallated platinum complexes **1–3**. Reagents and conditions: (a) i) *n*BuLi, THF, –78 °C, 1 h; ii) B(OCH<sub>3</sub>)<sub>3</sub>, –78 °C, 2 h, HCl; (b) 2-(4'-bromophenyl)pyridine, Na<sub>2</sub>CO<sub>3</sub>/[Pd(PPh<sub>3</sub>)<sub>4</sub>] (3.6 mol-%), toluene/H<sub>2</sub>O (3:1, v/v), Ar, 90 °C, 20 h; (c) i) [K<sub>2</sub>PtCl<sub>4</sub>], 2-ethoxyethanol/water (3:1, v/v), Ar, 80 °C, 20 h; ii) Hacac/Na<sub>2</sub>CO<sub>3</sub>, 2-ethoxyethanol, 100 °C, 20 h; (d) ethynyltrimethylsilane, [Pd(PPh<sub>3</sub>)Cl<sub>2</sub>] (2 mol-%), CuI (4 mol-%), PPh<sub>3</sub> (4 mol-%), NEt<sub>3</sub>/THF (3:1 v/v), Ar, 90 °C, 12 h; (e) K<sub>2</sub>CO<sub>3</sub>, MeOH/diethyl ether (2:1, v/v), room temp., 24 h; (f) 2-(4'-bromophenyl)pyridine, [Pd(PPh<sub>3</sub>)<sub>2</sub>Cl<sub>2</sub>] (2 mol-%), CuI (2 mol-%), PPh<sub>3</sub> (10 mol-%), NEt<sub>3</sub>/THF (3:5, v/v), Ar, 90 °C, 8 h.

## X-ray Crystal Structures

The crystal structures of **Pt-2** and **Pt-3** were determined. For **Pt-2**, half of the molecules in the crystal exist as head-to-head dimers with the coordination plane of the molecules parallel to each other. The Pt–Pt distance is 3.194 Å, which is within the range of 2.7–3.5 Å and thus a weak Pt<sup>II</sup>...Pt<sup>II</sup> interaction is possible in the crystal.<sup>[4,42]</sup>

The platinum atom resides in a square-planar geometry (Figure 1). The Pt–N distance is 1.995 Å, which is slightly longer than that of common Pt–N bonds. The Pt–O and Pt–C distances are in the range of 1.978–2.108 and 1.940–1.967 Å, respectively. The C–Pt–N and O–Pt–O angles are 82.5 and 93.2°, respectively, which are similar to reported values.<sup>[2,4]</sup>

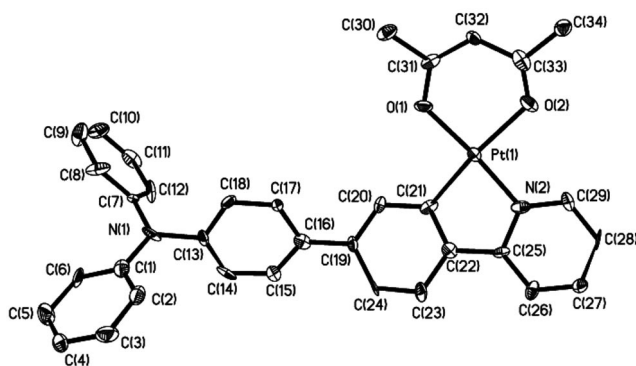


Figure 1. Perspective view of the crystal structure of **Pt-2** (30% probability ellipsoids, hydrogen atom labels have been omitted for clarity).

The crystal structure of the  $\alpha$ -diketo-containing **Pt-3** was also determined (Figure 2). In contrast to **Pt-2**, no dimer packing was found for **Pt-3**. The Pt<sup>II</sup>–Pt<sup>II</sup> distance is 6.782 Å; thus, no Pt<sup>II</sup>...Pt<sup>II</sup> interaction exists in **Pt-3**. This is probably due to the skewed geometry of the  $\alpha$ -diketo moiety [the torsion angle of O(3)–C(21)–C(20)–O(4) is 98.3°], which prevents tight packing of the molecules in the crystal. We found that the two carbonyl groups adopt a coplanar geometry with the connected aromatic moiety. For example, the O(3)–C(21)–C(22)–C(23) and O(4)–C(20)–C(17)–C(16) torsion angles are 176.8 and 13.7°, respectively. The Pt–C and Pt–N bond lengths are 1.958 and 1.990 Å, respectively. The C–Pt–N and O–Pt–O bond angles are 81.42 and 91.8°, respectively. These values are similar to those of **Pt-2**.

## UV/Vis Absorption Spectra of the Ligands and Complexes

The UV/Vis absorption behaviour of the ligands and complexes were studied (Figure 3). The absorptions at 350–400 nm are due to the  $\pi$ – $\pi^*$  transition in the TPA fragment. On metallation, the absorptions show a redshift of around 50 nm (Figure 3, b). A shoulder appeared at the red end of the spectra (beyond 400 nm); this weak absorption is the result of a spin-allowed <sup>1</sup>MLCT transition.<sup>[1,3]</sup> We noted that the molar extinction coefficient ( $\epsilon$ ) of **Pt-1** at around 420 nm is in the range of 20000–30000 dm cm<sup>−1</sup> mol<sup>−1</sup>. Such

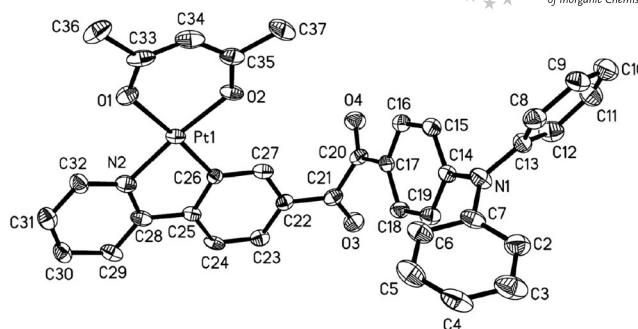


Figure 2. Perspective view of the crystal structure of **Pt-3** (30% probability ellipsoids, hydrogen atom labels have been omitted for clarity).

a high  $\epsilon$  value is beneficial for luminescent biosensing or bioimaging applications.<sup>[43]</sup> The absorption of **Pt-1** is redshifted relative to **L-1**, which is due to the cyclometallation of TPA and the MLCT absorption.

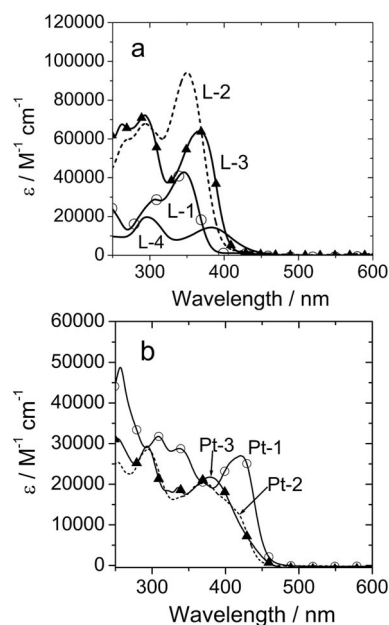


Figure 3. UV/Vis absorption spectra of (a) the ligands and (b) the Pt complexes;  $c = 1.0 \times 10^{-5}$  mol dm<sup>−3</sup> in dichloromethane. 25 °C.

## Photoluminescence Spectra of the Ligands and Complexes

The emission behaviour of the ligands and complexes were also studied (Figure 4). For the ligands, broad, structureless emission bands were observed. We found that **L-4** shows the longest wavelength emission (489 nm). These emissions are due to the S<sub>1</sub> state of the ligands and are of  $\pi$ – $\pi^*$  character.

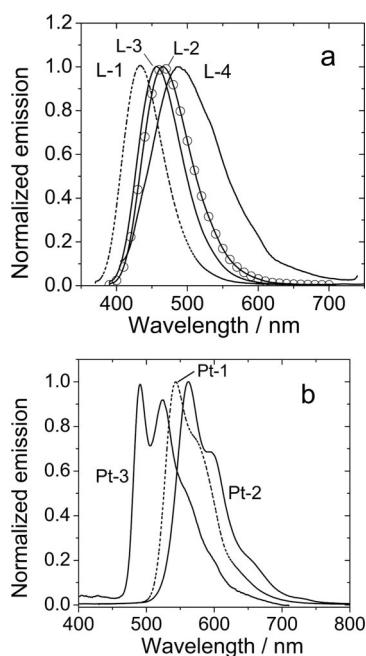


Figure 4. Emission spectra of (a) the ligands and (b) the Pt complexes;  $c = 1.0 \times 10^{-5} \text{ mol dm}^{-3}$  in dichloromethane, 25 °C.

For **Pt-1**, structured emission at 542 nm was observed; the profile is typical of cyclometallated Pt complexes.<sup>[1,3]</sup> The emission is red-shifted by 60 nm relative to the parent complex [ppyPt(acac)], which shows emission at 486 nm.<sup>[3]</sup> We propose that the red-shifted emission is due to the strong electron-donating ability of the diphenylamine group. The structured emission band, large Stokes shift and long luminescent lifetime (3.7  $\mu\text{s}$ ) infer that the emission at 542 nm is phosphorescent in nature. This emission colour tuning approach will be useful in the design of phosphorescent emitters.

Previously, **Pt-1** was reported as a fluorescence/phosphorescence dual emissive material,<sup>[4]</sup> but we observed only phosphorescence (Figure 4). We tentatively propose the discrepancy to be due to the highly sensitive nature of the emission of this complex to oxygen. Trace amounts of oxygen in the solution will diminish the emission and lead to a pseudo-dual emission (because the fluorescence emission will be relatively high and the fluorescence/phosphorescence emission intensity will become comparable).

For **Pt-2**, an emission band at around 561 nm was observed, which is red-shifted by about 80 nm relative to

[ppyPt(acac)]. For **Pt-3**, emission at 490 nm was observed. The large Stokes shifts and the emissions at red-shifted wavelengths suggest that the emission is due to the triplet excited state, that is, the emission is phosphorescent in nature. We propose the phosphorescence to be due to the  $^3\text{MLCT}/^3\text{IL}$  mixed excited state.<sup>[3,4,44,45]</sup>

The photophysical properties of the ligands and the Pt complexes are compiled in Table 1. The fluorescence quantum yields of the ligands are generally high and their fluorescence lifetimes are in the range of ns, which is in agreement with singlet emission. **Pt-1**, has a luminescent lifetime of 3.7  $\mu\text{s}$  at room temperature, which is longer than that of the parent complex [ppyPt(acac)] ( $\tau = 2.6 \mu\text{s}$ ).<sup>[3]</sup> The emission wavelength of **Pt-1** is red-shifted relative to that of [ppyPt(acac)], whereas the luminescent lifetimes are extended.

We found that the emission of the complexes is concentration-independent. For example, the emission profile of **Pt-1** does not change with increasing concentration (Figure 5). Similar results were observed for **Pt-2** (see the Supporting Information).

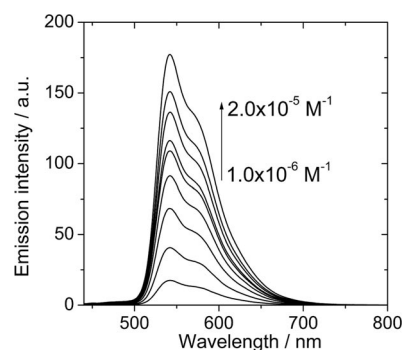


Figure 5. Emission of **Pt-1** in  $\text{CH}_2\text{Cl}_2$  solution at different concentrations;  $\lambda_{\text{ex}} = 425 \text{ nm}$ , 27 °C.

### DFT/TDDFT Calculations and the Low-Lying Excited States of the Complexes

Recently, density functional theory (DFT) calculation methods were successfully used to study the photophysics of fluorescent and phosphorescent chromophores.<sup>[43,46–52]</sup> The photophysics of lumophores can be better understood by revealing the electronic structures of the excited states.<sup>[2–4,18,19,43]</sup> In this work we carried out theoretical cal-

Table 1. Photophysical parameters of the platinum complexes **Pt-1**, **Pt-2** and **Pt-3** and the ligands.

	$\lambda_{\text{abs}}$ [nm] <sup>[a]</sup>	$\lambda_{\text{ex}}$ [nm]	$\lambda_{\text{em}}$ [nm]	$\Phi_{\text{f}}^{\text{[b]}}$	$\Phi_{\text{p}}^{\text{[c]}}$	$\tau$
<b>L-1</b>	307 (2.88), 346 (4.29)	364	433	0.8999	— <sup>[d]</sup>	3.34 ns
<b>L-2</b>	294 (6.79), 350 (9.45)	376	456	0.2562	— <sup>[d]</sup>	2.32 ns
<b>L-3</b>	294 (7.22), 367 (6.40)	388	466	0.6076	— <sup>[d]</sup>	2.07 ns
<b>L-4</b>	297 (1.97), 383 (1.44)	388	489	0.0008	— <sup>[d]</sup>	4.82 ns
<b>Pt-1</b>	308 (3.18), 338 (2.88), 420 (2.70)	425	542, 600	— <sup>[d]</sup>	0.36	3.70 $\mu\text{s}$
<b>Pt-2</b>	294 (2.86), 371 (2.23)	372	561, 596	— <sup>[d]</sup>	0.21	5.45 $\mu\text{s}$
<b>Pt-3</b>	293 (2.94), 336 (1.92), 377 (2.18)	376	490, 532	— <sup>[d]</sup>	0.03	3.07 $\mu\text{s}$

[a] Extinction coefficients ( $10^4 \text{ M}^{-1} \text{ cm}^{-1}$ ) are shown in parentheses. [b] Fluorescence quantum yield in aerated  $\text{CH}_2\text{Cl}_2$ . [c] Phosphorescence quantum yield in deaerated  $\text{CH}_2\text{Cl}_2$ . [d] Not applicable.

culations on the complexes and the photophysical properties, such as the excitation and emission properties, were investigated with time-dependent DFT (TDDFT) calculations. The main objective of the theoretical calculations was to investigate the electronic structures of the low-lying excited states and to correlate them with their emission properties. This information will be helpful in the future design of luminescent cyclometallated Pt complexes with predetermined photophysical properties such as red-shifted emission wavelengths or long luminescent lifetimes.<sup>[25]</sup>

The optimized ground-state geometry of **Pt-1** indicates a planar square-coordinated Pt centre with Pt–N and Pt–C bond lengths of 2.02 and 1.99 Å, respectively. These bond lengths are very similar to the values determined for the single-crystal structure of the cyclometallated Pt complex.<sup>[4]</sup>

The HOMO of **Pt-1** is localized on the TPA moiety and the LUMO is mainly distributed on the pyridine. The Pt atom contributes to both the HOMO and the LUMO (Figure 6). To assign the UV/Vis absorption and emission spectra, the vertical excitation energies of the complex were calculated with TDDFT on the basis of the ground-state geometry (Table 2).

The calculated UV/Vis absorption of the  $S_0 \rightarrow S_1$  transition is centred at 437 nm, which is in good agreement with the UV/Vis absorption at 420 nm (Figure 3). The  $S_1$  state is characterized by HOMO  $\rightarrow$  LUMO and HOMO-2  $\rightarrow$  LUMO transitions, both are assigned as TPA  $\rightarrow$  pyridine charge transitions. The Pt atom is involved in this transition (Figure 6). Other excited states, such as the  $S_{11}$  state (309 nm, due to the TPA localized excitation), correlate well with the experimental UV/Vis absorption at 308 nm (Figure 4). This assignment of the UV/Vis absorption is in agreement with the traditional understanding of the photophysics of these complexes, that is, MLCT/IL mixed transitions.<sup>[3]</sup>

The triplet states of **Pt-1** were also investigated. For the lowest-lying triplet excited state, that is,  $T_1$ , which is respon-

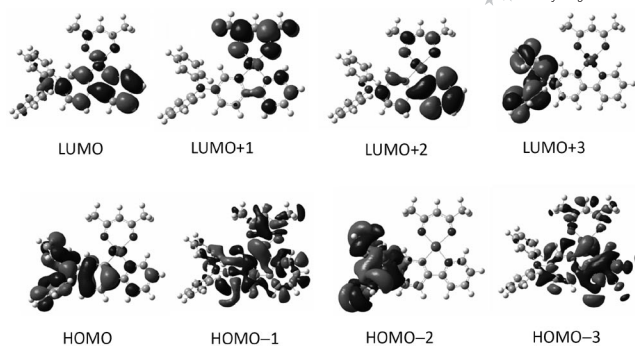


Figure 6. Selected frontier molecular orbitals of complexes **Pt-1** calculated by DFT at the B3LYP/6-31G(d)/LanL2DZ level of theory using Gaussian 09.

sible for the emission (Kasha's rule),<sup>[21,43,53]</sup> the electronic structure is characterized by HOMO  $\rightarrow$  LUMO and HOMO-2  $\rightarrow$  LUMO transitions, both are assigned as TPA  $\rightarrow$  pyridine ( $^3$ IL) and diphenylamine  $\rightarrow$  pyridine ( $^3$ IL) transitions. The Pt atom is also involved in these transitions. These pictures are in good agreement with the accepted photophysics of [ppyPt(acac)] complexes. The calculated excitation energy for the  $T_1$  excited state is 545 nm, which is consistent with the emission band observed at 542 nm.<sup>[54]</sup>

Note that the vertical excitation energies were calculated on the basis of the ground-state geometry of the complex. The agreement between the virtual  $S_0 \rightarrow T_1$  excitation energy and the experimental  $T_1 \rightarrow S_0$  emission energy infers that the geometry relaxation in the  $T_1$  excited state is not significant, probably due to the rigid structure of **Pt-1**.

Similar theoretical calculations were also carried out for **Pt-2** (Figure 7 and Table 3). First the geometries of the complex and the ligands were optimized. It was found that the dihedral angle between the TPA and the ppy groups is 33.8°. This value is very close to the torsion angle of 33.79°

Table 2. Electronic excitation energies and the corresponding oscillator strengths ( $f$ ), main configurations and CI coefficients of the low-lying electronically excited states of complex **Pt-1** calculated with TDDFT//B3LYP/6-31G(d)/LanL2DZ on the basis of the DFT//B3LYP/6-31G(d)/LanL2DZ-optimized ground-state geometries.

	Electronic transition	TDDFT//B3LYP/6-31G(d)				
		Energy <sup>[a]</sup>	$f$ <sup>[b]</sup>	Composition <sup>[c]</sup>	CI <sup>[d]</sup>	Character <sup>[e]</sup>
Singlet	$S_0 \rightarrow S_1$	2.84 eV, 437 nm	0.2998	H $\rightarrow$ L	0.6568	IL
				H-2 $\rightarrow$ L	0.1003	IL
	$S_0 \rightarrow S_2$	3.21 eV, 387 nm	0.0506	H $\rightarrow$ L	0.6422	IL
				H-2 $\rightarrow$ L	0.1974	IL
Triplet	$S_0 \rightarrow S_7$	3.69 eV, 336 nm	0.0707	H-2 $\rightarrow$ L	0.2920	IL
				H-1 $\rightarrow$ L+1	0.5994	MLCT
	$S_0 \rightarrow S_{11}$	4.01 eV, 309 nm	0.1700	H $\rightarrow$ L+3	0.6210	IL
	$S_0 \rightarrow T_1$	2.28 eV 545 nm	0.0000 <sup>[f]</sup>	H $\rightarrow$ L	0.6762	IL
				H-2 $\rightarrow$ L	0.1457	IL
				H $\rightarrow$ L+1	0.1137	LLCT
				H-1 $\rightarrow$ L	0.1114	MLCT
	$S_0 \rightarrow T_2$	2.84 eV, 437 nm	0.0000 <sup>[f]</sup>	H-1 $\rightarrow$ L+1	0.4873	MLCT
			H-2 $\rightarrow$ L+1	0.3669	LLCT	

[a] Only the selected low-lying excited states are presented. [b] Oscillator strength. [c] H represents the HOMO and L represents the LUMO. Only the main configurations are presented. [d] The CI coefficients are absolute values. [e] IL: intraligand; LLCT: ligand-to-ligand charge transfer; MLCT: metal-to-ligand charge transfer. [f] No spin-orbital coupling effect was considered, thus the  $f$  value is zero.

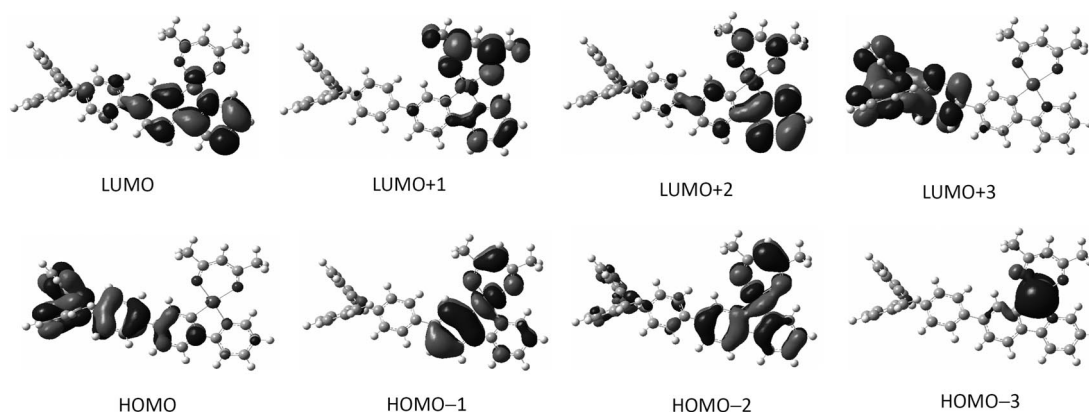


Figure 7. Frontier molecular orbitals for **Pt-2** calculated by DFT at the B3LYP/6-31G(d)/LanL2DZ level of theory using Gaussian 09.

Table 3. Electronic excitation energies and the corresponding oscillator strengths ( $f$ ), main configurations and CI coefficients of the low-lying electronically excited states of complex **Pt-2** calculated with TDDFT//B3LYP/6-31G(d)/LanL2DZ on the basis of the DFT//B3LYP/6-31G(d)/LanL2DZ-optimized ground-state geometries.

	Electronic transition	TDDFT//B3LYP/6-31G(d)				
		Energy <sup>[a]</sup>	$f$ <sup>[b]</sup>	Composition <sup>[c]</sup>	CI <sup>[d]</sup>	Character <sup>[e]</sup>
Singlet	$S_0 \rightarrow S_1$	2.80 eV, 444 nm	0.4071	H $\rightarrow$ L	0.6767	IL/LMCT
	$S_0 \rightarrow S_2$	3.07 eV, 404 nm	0.0174	H-4 $\rightarrow$ L	0.1227	IL/LLCT
	$S_0 \rightarrow S_3$	3.35 eV, 370 nm	0.0710	H-1 $\rightarrow$ L	0.6428	LLCT/MLCT
				H-2 $\rightarrow$ L	0.1333	LLCT/MLCT
	$S_0 \rightarrow S_6$	3.50 eV, 354 nm	0.0795	H $\rightarrow$ L+1	0.675	LLCT/LMCT
	$S_0 \rightarrow S_{17}$	4.21 eV, 295 nm	0.0705	H-2 $\rightarrow$ L	0.2043	LLCT/MLCT
				H $\rightarrow$ L+2	0.6468	LLCT/IL
Triplet	$S_0 \rightarrow T_1$	2.34 eV, 530 nm	0.0000 <sup>[f]</sup>	H-7 $\rightarrow$ L	0.2887	IL/LLCT
				H-4 $\rightarrow$ L	0.2389	IL/LLCT
				H-2 $\rightarrow$ L+2	0.5079	LLCT/MLCT
				H-4 $\rightarrow$ L	0.1444	IL/LLCT
	$S_0 \rightarrow T_2$	2.76 eV, 449 nm	0.0000 <sup>[f]</sup>	H-2 $\rightarrow$ L	0.2760	LLCT/MLCT
				H-1 $\rightarrow$ L	0.2792	LLCT/MLCT
				H $\rightarrow$ L	0.5627	LLCT/LMCT
				H $\rightarrow$ L+4	0.1359	LLCT/LMCT
				H-2 $\rightarrow$ L	0.1618	LLCT/MLCT
				H-1 $\rightarrow$ L	0.5815	LLCT/MLCT
				H $\rightarrow$ L	0.2631	IL/LMCT

[a] Only the selected low-lying excited states are presented. [b] Oscillator strength. [c] H represents the HOMO and L represents the LUMO. Only the main configurations are presented. [d] The CI coefficients are absolute values. [e] IL: intraligand; LLCT: ligand-to-ligand charge transfer; MLCT: metal-to-ligand charge transfer. [f] No spin-orbital coupling effect was considered, thus the  $f$  values are zero.

determined in the single-crystal structure analysis (Figure 1). The optimized O–Pt–O and C–Pt–N bond angles are 89.6 and 81.2°, respectively. The bond lengths of C–Pt and Pt–N are 1.991 and 2.018 Å, respectively. These values are close to the values determined in the single-crystal structure analysis. The calculated UV/Vis absorptions in the visible range are mainly due to the  $S_0 \rightarrow S_1$  (444 nm),  $S_0 \rightarrow S_2$  (404 nm) and  $S_0 \rightarrow S_3$  transitions (370 nm; Table 3). These absorption maxima are in good agreement with the experimental results (412 and 371 nm). Based on the orbitals involved in the transitions (Figure 7) we conclude that the transitions are mainly TPA  $\rightarrow$  ppy <sup>1</sup>IL and Pt  $\rightarrow$  ppy <sup>3</sup>MLCT excitations. The Pt  $\rightarrow$  ppy <sup>1</sup>MLCT transition is found for the  $S_2$  state (Table 3).

We found that the  $T_1$  state of **Pt-2** is comprised mainly of the HOMO  $\rightarrow$  LUMO transition. The Pt atom contributes slightly to this transition. Therefore it was proposed that

the triplet state will have a long lifetime due to the weak spin-orbital coupling effect of the Pt metal.<sup>[1,3]</sup> This is in agreement with the experimental observations, that is, luminescent lifetimes of 3.7 and 5.5  $\mu$ s were observed for **Pt-1** and **Pt-2**, respectively (Table 1).

Similar calculations were performed on **Pt-3** (Figure 8 and Table 4). We found that the  $\alpha$ -diketo moiety adopts a *trans* skewed geometry in the ground state with a torsion angle of 123.8°. The DFT optimization indicates that the two carbonyl groups adopt a coplanar geometry with the respective aromatic moieties to which the carbonyl groups are attached; the torsion angles are 0.36 and 1.16°, respectively. The calculated excitations with significant oscillator strengths are the excited states of  $S_6$ ,  $S_9$  and  $S_{20}$  with excitation energies of 372, 337 and 298 nm. These values are in good agreement with the experimental observations of 377, 336 and 293 nm, respectively (Figure 1).

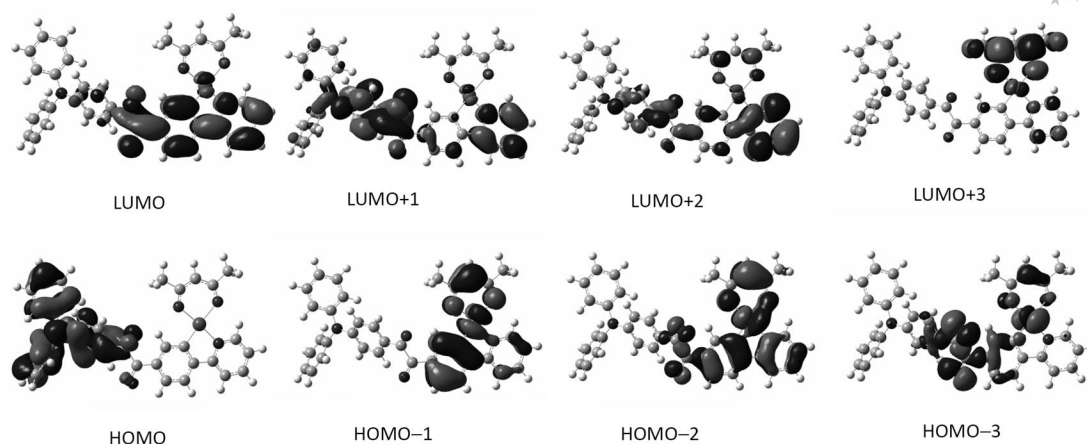


Figure 8. Frontier molecular orbitals for **Pt-3** calculated by DFT at the B3LYP/6-31G(d)/LanL2DZ level of theory using Gaussian 09.

Table 4. Electronic excitation energies and the corresponding oscillator strengths ( $f$ ), main configurations and CI coefficients of the low-lying electronically excited states of complex **Pt-3** calculated with TDDFT//B3LYP/6-31G(d)/LanL2DZ on the basis of the DFT//B3LYP/6-31G(d)/LanL2DZ-optimized ground-state geometries.

	Electronic transition	TDDFT//B3LYP/6-31G(d)				
		Energy <sup>[a]</sup>	$f^{[b]}$	Composition <sup>[c]</sup>	CI <sup>[d]</sup>	Character <sup>[e]</sup>
Singlet	$S_0 \rightarrow S_1$	2.65 eV, 467 nm	0.0374	H $\rightarrow$ L H-3 $\rightarrow$ L	0.6767 0.3456	IL/LMCT IL/LLCT
	$S_0 \rightarrow S_6$	3.33 eV, 372 nm	0.4274	H $\rightarrow$ L+1 H-3 $\rightarrow$ L+1	0.5925 0.2092	IL IL/MLCT/LLCT
	$S_0 \rightarrow S_9$	3.68 eV, 337 nm	0.0843	H $\rightarrow$ L+2 H-1 $\rightarrow$ L+2	0.6698 0.1407	IL/LLCT LLCT/MLCT
	$S_0 \rightarrow S_{20}$	4.16 eV, 298 nm	0.1806	H $\rightarrow$ L+6 H $\rightarrow$ L+5	0.4690 0.3617	IL IL
	Triplet	$S_0 \rightarrow T_1$	2.23 eV, 557 nm	0.0000 <sup>[f]</sup>	H-3 $\rightarrow$ L	0.4661
H-3 $\rightarrow$ L+1					0.2703	IL/LLCT/MLCT
H-2 $\rightarrow$ L					0.2517	LLCT/MLCT
$S_0 \rightarrow T_2$		2.33 eV, 531 nm	0.0000 <sup>[f]</sup>	H $\rightarrow$ L	0.2973	IL/LMCT
				H $\rightarrow$ L+1	0.2090	IL
				H-2 $\rightarrow$ L	0.3530	LLCT/MLCT
				H-1 $\rightarrow$ L	0.5857	IL/LLCT

[a] Only the selected low-lying excited states are presented. [b] Oscillator strength. [c] H represents the HOMO and L represents the LUMO. Only the main configurations are presented. [d] The CI coefficients are given as absolute values. [e] IL: intraligand; LLCT: ligand-to-ligand charge transfer; MLCT: metal-to-ligand charge transfer. [f] No spin-orbital coupling effect was considered, thus the  $f$  values are zero.

The  $S_0 \rightarrow T_1$  transition of **Pt-3** was found to have an excitation energy of 557 nm, which is very close to the phosphorescence emission (532 and 490 nm).<sup>[54]</sup> We found that the  $T_1$  state is characterized by TPA  $\rightarrow$  ppy/diketo ( $^3$ IL), Pt  $\rightarrow$  ppy/diketo ( $^3$ MLCT) and diketo  $\rightarrow$  localized  $^3$ IL transitions.

For electroluminescence, the energies of the HOMO and LUMO of the phosphorescent dopants are important for device fabrication.<sup>[4]</sup> The HOMO and LUMO energies calculated for the parent complex [ppyPt(acac)] are  $-5.41$  and  $-1.58$  eV, respectively. With electron-donating substitution on the ppy ligand, the HOMO and LUMO energies of **Pt-1** were calculated to be  $-4.76$  and  $-1.53$  eV, respectively. Thus, the LUMO energy is hardly affected but the energy of the HOMO is significantly increased with electron-donating substitution on the phenyl group of the ppy fragment. Thus, the energy gap is smaller and red-shifted emission is observed for **Pt-1** relative to that of [ppyPt(acac)]. The red-

shifted emission of **Pt-2** can be rationalized similarly. The HOMO and LUMO energies of **Pt-2** were calculated to be  $-4.79$  and  $-1.66$  eV, respectively.

For **Pt-3**, however, an electron-withdrawing  $\alpha$ -diketo group is attached to the phenyl fragment of the ppy ligand. Based on the traditional theory of the structure-emission properties of cyclometallated Pt complexes,<sup>[1,3]</sup> blue-shifted emission should be expected for **Pt-3** relative to that of [ppyPt(acac)]. Interestingly, red-shifted emission was observed for **Pt-3**. We found that the  $\alpha$ -diketo moiety is significantly involved in the LUMO (Figure 8) and thus we expect the energy of the LUMO to be reduced, that is, the  $\alpha$ -diketo moiety may act as an electron trap to perturb the electronic structure of the excited state of **Pt-3** (Figure 8). The HOMO energy of **Pt-3** ( $-5.20$  eV) is similar to that of [ppyPt(acac)] ( $-5.41$  eV), but the LUMO energy of **Pt-3** ( $-2.51$  eV) is significantly lower than that of [ppyPt(acac)] ( $-1.58$  eV). Thus, the HOMO-LUMO energy gap of **Pt-3** is much smaller

than that of [ppyPt(acac)] and therefore red-shifted emission is expected for **Pt-3**. This theoretical prediction is fully proven by the experimental results. Thus, the  $\alpha$ -diketo moiety acts as an efficient electron trap to perturb the excited state of cyclometallated Pt complexes thereby leading to red-shifted emission.<sup>[2]</sup> Tuning the emission wavelength of cyclometallated Pt complexes with an electron trap is rarely reported.<sup>[2]</sup> Our finding of  $\alpha$ -diketo as a new and efficient electron trap for this purpose may prove significant in the future molecular design of cyclometallated Pt complexes.

### Luminescent Oxygen Sensing

Recently, luminescent O<sub>2</sub> sensing has attracted considerable attention.<sup>[20,23,24,55–57]</sup> Usually Ru<sup>II</sup>-polypyridine or Pt<sup>II</sup>-porphyrin complexes are used for oxygen sensing. To the best of our knowledge no cyclometallated Pt(acac) complexes have been studied for O<sub>2</sub> sensing.<sup>[24]</sup> Thus, we carried out an investigation of the luminescent O<sub>2</sub>-sensing properties of the complexes **Pt-1**, **Pt-2** and **Pt-3**.

First we studied the luminescent O<sub>2</sub>-sensing properties of **Pt-2** in solution (Figure 9). We found that the phosphorescence emission band at 560 nm can be significantly quenched by O<sub>2</sub>. For example, the emission is significantly quenched with 0.04% O<sub>2</sub> (mixture with N<sub>2</sub>, v/v). The emission is almost completely quenched with 1.5% O<sub>2</sub>. A similar quenching effect was observed for **Pt-1** (see the Supporting Information).

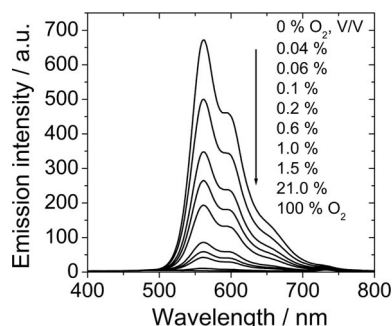


Figure 9. Emission spectra of complex **Pt-2** under different partial pressures of O<sub>2</sub> ( $\lambda_{\text{ex}} = 372$  nm, 12 °C).

We noted that the O<sub>2</sub> sensitivity of the emission of **Pt-3** towards O<sub>2</sub> is lower than that of **Pt-2**. This is consistent with the fact that **Pt-2** has longer luminescent lifetimes (Table 1).

### Luminescent O<sub>2</sub> Sensing of the Pt<sup>II</sup> Complexes in Polymer Films

For practical applications, the study of sensing films, for example, prepared by the distribution of complexes in supporting polymers, is more meaningful than the study of oxygen-sensing in solution. Thus, the O<sub>2</sub>-sensing properties of the complexes were also studied in polymer films (IMPEK-C; Figure 10).<sup>[20,21,23,25,58,59]</sup>

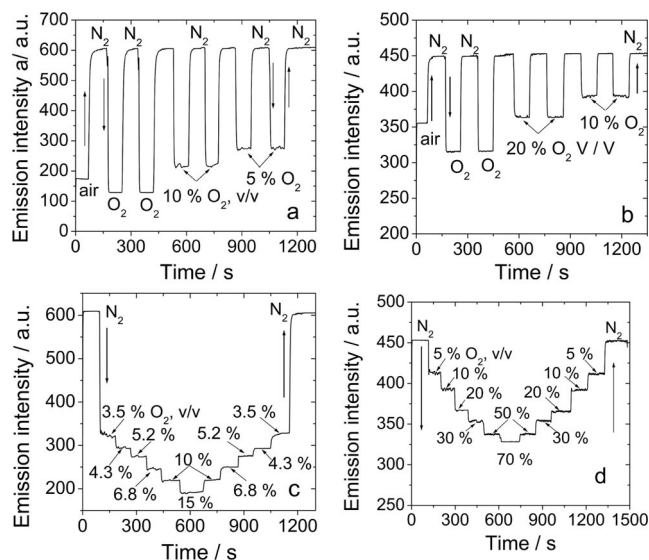


Figure 10. Phosphorescent intensity response of sensing films of the complexes in IMPEK-C to saturation O<sub>2</sub>/N<sub>2</sub> cycles and small-step variations of O<sub>2</sub> concentrations. (a) Saturation switching and (c) dynamic emissive intensity response of sensing films of **Pt-1** in IMPEK-C to O<sub>2</sub>/N<sub>2</sub> saturation cycles.  $\lambda_{\text{ex}} = 400$  nm,  $\lambda_{\text{em}} = 535$  nm, 33 °C. (b) Saturation switching and (d) dynamic emissive intensity response of **Pt-3** in IMPEK-C to O<sub>2</sub>/N<sub>2</sub> saturation cycles.  $\lambda_{\text{ex}} = 372$  nm,  $\lambda_{\text{em}} = 540$  nm, 30 °C.

For heterogeneous O<sub>2</sub>-sensing films, a modified Stern–Volmer or a two-site model is required to study the quenching effect.<sup>[20,23,24]</sup> In the two-site model, the O<sub>2</sub>-sensitive dyes are considered as two different portions. The fraction of the two portions are defined as  $f_1$  and  $f_2$ , respectively ( $f_1 + f_2 = 1$ ); the two portions have different quenching constants ( $K_{\text{SV}1}$  and  $K_{\text{SV}2}$ ); see Eq. (1).

$$\frac{I_0}{I} = \frac{1}{\frac{f_1}{1 + K_{\text{SV}1}P_{\text{O}_2}} + \frac{f_2}{1 + K_{\text{SV}2}P_{\text{O}_2}}} \quad (1)$$

With the home-assembled flow cell coupled to a spectrofluorimeter, the responses of the sensing films to different O<sub>2</sub> partial pressure were studied (Figure 10). First the O<sub>2</sub>-sensing films of **Pt-1** and **Pt-3** were tested against the saturation cycle of O<sub>2</sub> and N<sub>2</sub> (Figure 10, a and b). The films in N<sub>2</sub> exhibit intense emission, but the phosphorescence is substantially quenched in O<sub>2</sub>. Furthermore, fast response ( $t_{\downarrow 95}$ ) and recovery times ( $t_{\uparrow 95}$ ) of 2 and 6 s were observed, respectively.<sup>[20,25]</sup> The response ( $t_{\downarrow 95}$ ) and recovery times ( $t_{\uparrow 95}$ ) are generally accepted as the times for luminescence intensity changes to reach 95% of the whole variation when switching from 100% N<sub>2</sub> to 100% O<sub>2</sub> or vice versa. **Pt-2** is also sensitive towards O<sub>2</sub> (see the Supporting Information). Fast response times are usually observed for porous supporting materials such as MCM-41 molecular sieves.<sup>[2,60–64]</sup> However, our polymer film preparation approach is straightforward.

Next, the dynamic response of the O<sub>2</sub>-sensing films was tested against small steps of O<sub>2</sub> partial pressure variation

(Figure 10, c and d). Such a detailed study will reveal the dynamic  $O_2$  partial pressure range and the data can be used to evaluate  $O_2$  sensitivity.<sup>[20,25]</sup> We found that the sensing film of **Pt-1** is more sensitive to  $O_2$  than **Pt-3**. For example, the emission intensity of **Pt-1** was quenched by 68.6% under 3.5%  $O_2$ . For **Pt-3**, however, the emission is quenched by only around 9% in the presence of 5%  $O_2$ . To compare the  $O_2$ -sensing properties of the complexes quantitatively, the  $O_2$ -sensing data were fitted to the two-site model (Figure 11) and the results are summarized in Table 5. We can clearly see the apparent quenching constants (the sensitivity towards  $O_2$ ) of the complexes **Pt-1** ( $K_{SV}^{app} = 0.045 \text{ Torr}^{-1}$ ) and **Pt-2** ( $0.030 \text{ Torr}^{-1}$ ) are nearly 10-fold higher than that of the complex of **Pt-3** ( $0.003 \text{ Torr}^{-1}$ ). This result shows that the luminescence lifetime of **Pt-3** is shorter than those of the complexes of **Pt-1** and **Pt-2**, which is supported by the experimental results (Table 1).

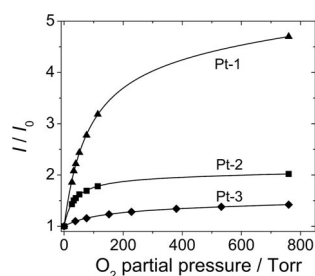


Figure 11. Two-site model plots for the sensing films of **Pt-1**, **Pt-2** and **Pt-3** in IMPEK-C. Intensity ratios  $I/I_0$  vs.  $O_2$  partial pressure.

Table 5. Parameters for the  $O_2$ -sensing film of complexes **Pt-1**, **Pt-2** and **Pt-3** with IMPEK-C as the supporting matrix (fitting of the results to the two site model).

	$f_1^{[a]}$	$f_2^{[a]}$	$K_{SV1}^{[b]}$	$K_{SV2}^{[b]}$	$r^{2[c]}$	$K_{SV}^{app[d]}$	$pO_2^{[e]}$
<b>Pt-1</b>	0.7891	0.2109	0.0564	0.0001	1.000	0.04453	22.5
<b>Pt-2</b>	0.5001	0.4999	0.0601	0.0000	0.999	0.03006	33.3
<b>Pt-3</b>	0.2898	0.7102	0.0112	0.0001	1.000	0.00332	301.5

[a] Ratio of the two portions of dyes. [b] Quenching constants of the two portions. [c] Determination coefficients. [d] Weighted quenching constant,  $K_{SV}^{app} = f_1 K_{SV1} + f_2 K_{SV2}$ . [e] The oxygen partial pressure at which the initial emission intensity of the film is quenched by 50% and calculated as  $1/K_{SV}$ . In Torr

### Electroluminescent Properties

As a preliminary investigation, the electroluminescence properties of **Pt-2** and **Pt-3** were studied by using the complexes as dopants in the emission layer of OLEDs (Figure 12).<sup>[4]</sup>

The EL spectra of the devices based on complexes **Pt-2** and **Pt-3** at different doping concentration are shown in Figure 13. For the devices based on **Pt-2** (Figure 13, a), the emission at 548 nm is due to monomer emission and the band at around 590 nm is assigned to excimer emission. The EL spectra of the complexes changed with doping concentration as a result of excimer emission. The excimer emission increases in intensity with increasing doping concen-

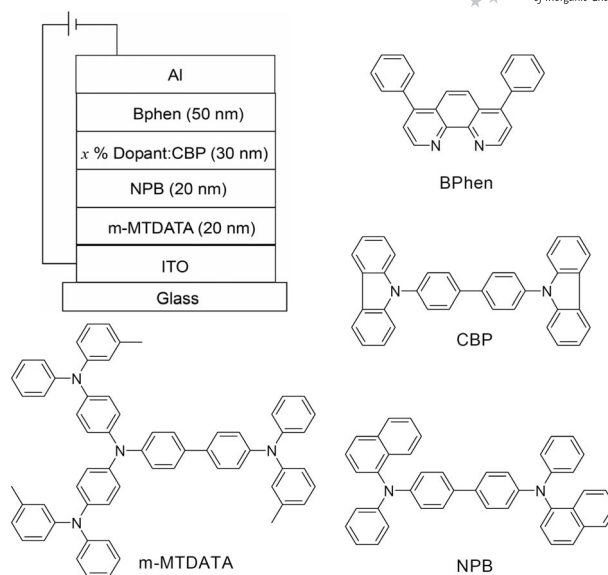


Figure 12. The configuration of the electrophosphorescent OLED devices and the structures of the compounds used in the devices.

tration. The emission at around 413 nm derives from NPB {4,4'-bis[(1-naphthyl)phenylamino]biphenyl} and increases in intensity with decreasing doping concentration.

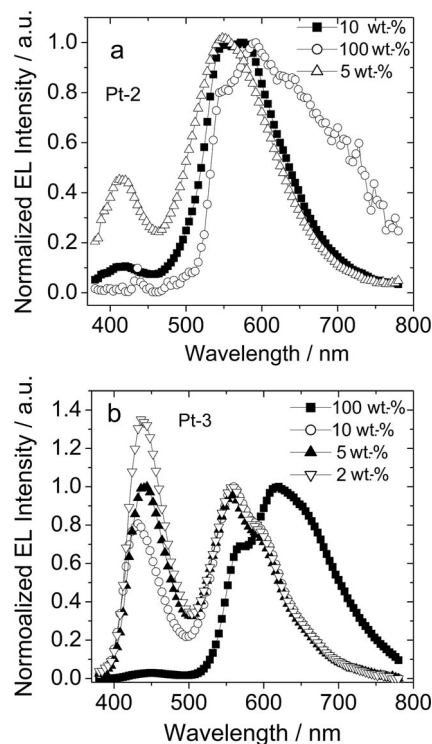


Figure 13. EL spectra of OLED devices using (a) **Pt-2** and (b) **Pt-3** as dopants at different doping concentrations.

For the devices based on **Pt-3** (Figure 13, b), the emission at around 559 nm is assigned to the monomer and the band at around 618 nm is assigned to excimer emission. The emission at around 430 nm derives from NPB and the intensity increases with decreasing doping concentration. The emission peak from NPB exhibits a small blueshift with in-

creasing doping concentration due to the absorption of complex **Pt-3**. The device based on complex **Pt-3** emits pure white light with CIE coordinates ( $x, y$ ) of (0.32, 0.32) at the 5 wt.-% doping ratio under 12 V.

The current density–luminance ( $J$ – $L$ ) and  $J$  current efficiency characteristics of the devices based on the complexes **Pt-2** and **Pt-3** were also studied (see the Supporting Information). The devices based on **Pt-2** and **Pt-3** show a different dependence on doping concentration. For **Pt-2**, the device with 10 wt.-% doping concentration exhibits a much better performance than that with a 5 wt.-% doping concentration. The 10 wt.-%-doped device has a turn-on voltage of 6 V and a maximum luminance ( $L_{\text{max}}$ ) of 1298  $\text{Cd m}^{-2}$  at a current density of 374  $\text{mA cm}^{-2}$ . The maximum luminance efficiency is 3.96  $\text{Cd A}^{-1}$  at  $J = 183 \text{ mA cm}^{-2}$ . In contrast, for **Pt-3**, the device with 5 wt.-% doping concentration shows a better performance than that with 10 and 2 wt.-% doping concentrations. The 5 wt.-%-doped device has a turn-on voltage of 6 V and a maximum luminance of 1931  $\text{Cd m}^{-2}$  at a current density of 180.4  $\text{mA cm}^{-2}$ . The maximum luminance efficiency is 1.86  $\text{Cd A}^{-1}$  at  $J = 35 \text{ mA cm}^{-2}$ . This phenomenon suggests that the device with **Pt-3** as the phosphorescent dopant is more prone to concentration saturation than that with **Pt-2**.

## Conclusions

Triphenylamine (TPA)-substituted [ppyPt(acac)] (ppy = 2-phenylpyridine, acac = acetylacetonato) complexes with different linkers between the TPA and the ppy moiety have been prepared. The TPA fragment is either directly cyclometallated (**Pt-1**) or attached to the ppy ligand through a C–C single bond (**Pt-2**) or a  $\alpha$ -diketo group (**Pt-3**). All the complexes show red-shifted room-temperature phosphorescence emission (centred at ca. 530–590 nm) relative to the parent complex [ppyPt(acac)] (emission at 486 nm). Through DFT calculations, the red-shifted emission of the complexes **Pt-1** and **Pt-2** can be rationalized by their higher HOMO energies, whereas a lower LUMO energy was found for **Pt-3** (due to the electron trap effect of the  $\alpha$ -diketo fragment); in each case there is a reduced HOMO–LUMO energy gap and red-shifted emission. The phosphorescence of the complexes show extended luminescence lifetimes (3.0–5.5  $\mu\text{s}$ ) compared with the parent complex [ppyPt(acac)] ( $\tau_{\text{phos}} = 2.6 \mu\text{s}$ ). The complexes were successfully used for luminescent  $\text{O}_2$  sensing and the  $\text{O}_2$  sensitivity can be varied by 13-fold (Stern–Volmer quenching constants). White light emission was observed with the OLED fabricated with **Pt-3** with CIE coordinates of (0.32, 0.32). Our study of these phosphorescent cyclometallated Pt complexes and their luminescent  $\text{O}_2$  sensing and electroluminescent properties will be useful in the design of new phosphorescent complexes for application as luminescent oxygen-sensing or OLED materials.

## Experimental Section

The chemicals used in the syntheses were analytically pure and were used as received without further purification. Solvents were prop-

erly dried or distilled before use in the syntheses and spectroscopic studies. NMR spectra were recorded with a 400 MHz Varian Unity Inova spectrometer. Mass spectra were recorded with a Q-TOF Micro spectrometer. Uv/vis absorption spectra were recorded with a HP8453 Uv/vis spectrophotometer. Fluorescence spectra were recorded with a JASCO FP-6500 or Sanco 970 CRT spectrofluorimeter. Luminescent quantum yields were measured with [Ru(bpy)<sub>2</sub>(phen)] as reference ( $\Phi = 6.0\%$ , in  $\text{CH}_3\text{CN}$ , under deaerated conditions). Luminescent lifetimes were measured with a Horiba Jobin Yvon Fluoro Max-4 (TCSPC) instrument.

**DFT/TDDFT Calculations:** The structures of the complexes were optimized using density functional theory (DFT) with the B3LYP functional and 6-31G(d)/LanL2DZ basis set. The vertical excitation energies were calculated with time-dependent DFT (TDDFT) on the basis of the optimized ground-state geometries. The 6-31G (d) basis set was employed for C, H, N, O and the LanL2DZ basis set was used for Pt<sup>II</sup>. There are no imaginary frequencies for any of the optimized structures. All these calculations were performed with the Gaussian 09 software package.<sup>[65]</sup>

**X-ray Structural Analysis:** Single-crystal X-ray diffraction data were obtained with a Bruker SMART APEX CCD diffractometer using graphite-monochromated Mo- $K_{\alpha}$  radiation ( $\lambda = 0.71073 \text{ \AA}$ ) with the SMART and SAINT programs. The data were collected using the  $\omega/2\theta$  scan mode and corrected for Lorentzian and polarization effects during the data reduction using SHELXTL 97 software the absorption effect was corrected for as well.<sup>[66]</sup>

CCDC-762460 (for **Pt-2**) and -762459 (for **Pt-3**) contain the supplementary crystallographic data for this paper. These data can be obtained free of charge from The Cambridge Crystallographic Data Centre via [www.ccdc.cam.ac.uk/data\\_request/cif](http://www.ccdc.cam.ac.uk/data_request/cif).

**Synthesis of 2-(4'-Bromophenyl)pyridine:**<sup>[7]</sup> At 0 °C,  $\text{NaNO}_2$  (4.14 g, 0.06 mmol, 8.0 M solution in water) was slowly added to a suspension of *p*-bromoaniline (5.00 g, 0.03 mmol, 1 equiv.) in concentrated HCl (10 mL). The mixture was stirred for 1 h at 0 °C and then added dropwise into pyridine (125 mL). The brown solution was stirred at 40 °C for 4 h and then  $\text{Na}_2\text{CO}_3$  (50.0 g) was added. The slurry was stirred at the same temperature for a further 18 h. The mixture was extracted with  $\text{CH}_2\text{Cl}_2$  ( $3 \times 50 \text{ mL}$ ) and the combined organic layers were dried with  $\text{Na}_2\text{SO}_4$  and the solvents evaporated to dryness. The crude product was purified with column chromatography (silica gel, toluene/MeOH = 95:5, v/v). An orange solid was obtained; yield 1.64 g, 23.0%. <sup>1</sup>H NMR (400 MHz,  $\text{CDCl}_3$ ):  $\delta = 8.68$  (d,  $J = 4.0 \text{ Hz}$ , 1 H), 7.86 (d,  $J = 8.4 \text{ Hz}$ , 2 H), 7.77 (t,  $J = 6.4 \text{ Hz}$ , 1 H), 7.73 (d,  $J = 8.4 \text{ Hz}$ , 1 H), 7.58 (d,  $J = 8.4 \text{ Hz}$ , 2 H), 7.25 (t,  $J = 6.0 \text{ Hz}$ , 1 H) ppm. HRMS (EI): calcd. for  $\text{C}_{11}\text{H}_8\text{NBr}$  [M]<sup>+</sup> 232.9840; found 232.9849.

**Synthesis of 4-Bromotriphenylamine:**<sup>[67]</sup> Triphenylamine (5.00 g, 20.4 mmol) in DMF (25 mL) was stirred at room temperature and then *N*-bromosuccinimide (NBS, 3.60 g, 20.4 mmol) in DMF (25 mL) was added in small portions. After stirring overnight at room temp., the reaction mixture was poured into water and extracted with diethyl ether. The organic layer was dried with anhydrous  $\text{Na}_2\text{SO}_4$ . After removing the solvent by evaporation, the crude white solid was purified by recrystallization from methanol. A white solid was obtained; yield 3.86 g, 59.5%. <sup>1</sup>H NMR (400 MHz,  $\text{CDCl}_3$ ):  $\delta = 7.31$  (d,  $J = 8.8 \text{ Hz}$ , 2 H), 7.24–7.28 (m, 4 H), 7.02–7.10 (m, 6 H), 6.93 (d,  $J = 9.2 \text{ Hz}$ , 2 H) ppm. HRMS (EI): calcd. for  $\text{C}_{18}\text{H}_{14}\text{NBr}$  [M]<sup>+</sup> 323.0310; found 323.0320.

**Synthesis of 4-(Diphenylamino)-1-phenylboronic Acid:**<sup>[68]</sup> A solution of 4-bromotriphenylamine (6.00 g, 18.5 mmol) in THF (40 mL) was cooled to  $-78 \text{ }^\circ\text{C}$  under Ar. *n*BuLi (2.5 M solution in hexane,

9.0 mL, 22.5 mmol) was added slowly through a syringe. The mixture was stirred for 1 h at  $-78^{\circ}\text{C}$ . Then  $\text{B}(\text{OMe})_3$  (2.34 g, 2.5 mL, 22.5 mmol) was added quickly through a syringe. The reaction mixture was stirred for a further 2 h before being allowed to warm to room temperature. Aqueous  $\text{HCl}$  (5.0%) was added to bring the pH to 5–6. Then the mixture was extracted with  $\text{CH}_2\text{Cl}_2$  ( $3 \times 50$  mL). The combined organic phase was washed with water (100 mL) and brine (100 mL). Then the organic phase was dried with anhydrous  $\text{Na}_2\text{SO}_4$  and the solvents were removed. A white powder was obtained; yield 4.47 g, 83.0%.  $^1\text{H}$  NMR analysis was performed on the 2,2-dimethylpropane-1,3-diol-protected 4-(diphenylamino)phenylboronic acid:  $^1\text{H}$  NMR (400 MHz,  $\text{CDCl}_3$ ):  $\delta$  = 7.64 (d,  $J$  = 8.4 Hz, 2 H), 7.22–7.26 (m, 4 H), 7.09 (d,  $J$  = 7.6 Hz, 4 H), 7.02–7.04 (m, 4 H), 3.75 (s, 4 H), 1.02 (t,  $J$  = 7.6 Hz, 6 H) ppm. HRMS (EI): calcd. for  $\text{C}_{23}\text{H}_{24}\text{BNO}_2$   $[\text{M}]^+$  357.1900; found 357.1909.

***N,N*-Diphenyl-4-(2-pyridinyl)benzeneamine (L-1)**:<sup>[69]</sup> 2-Bromopyridine (0.240 g, 1.53 mmol), triphenyl boronic acid (0.49 g, 1.68 mmol),  $[\text{Pd}(\text{PPh}_3)_4]$  (88.5 mg, 0.086 mmol),  $\text{K}_2\text{CO}_3$  (2.76 g, 2.0 M aqueous solution, 10 mL) and toluene (15 mL) were mixed. The mixture was degassed and heated at reflux at  $90^{\circ}\text{C}$  for 20 h under Ar. After being cooled, the solvent was evaporated under reduced pressure, the organic product was extracted with  $\text{CH}_2\text{Cl}_2$ , dried with  $\text{Na}_2\text{SO}_4$  and then evaporated to dryness. The crude product was purified by column chromatography (silica gel,  $\text{CH}_2\text{Cl}_2$ /petroleum ether = 2:1, v/v). A light-yellow solid was obtained; yield 0.22 g, 44.0%.  $^1\text{H}$  NMR (400 MHz,  $\text{CDCl}_3$ ):  $\delta$  = 8.63 (d,  $J$  = 4.8 Hz, 1 H), 7.85 (d,  $J$  = 8.8 Hz, 2 H), 7.70–7.63 (m, 2 H), 7.26 (t,  $J$  = 8.4 Hz, 2 H), 7.12–7.15 (m, 6 H), 7.03 (t,  $J$  = 7.2 Hz, 2 H) ppm. HRMS (EI): calcd. for  $\text{C}_{23}\text{H}_{18}\text{N}_2$   $[\text{M}]^+$  322.1470; found 322.1472.

**Pt-1**:<sup>[4]</sup> Under Ar, **L-1** (0.17 g, 0.527 mmol) and  $[\text{K}_2\text{PtCl}_4]$  (109.0 mg, 0.26 mmol) were added to a mixture of 2-ethoxyethanol (6 mL) and water (2 mL). The suspension was heated at  $80^{\circ}\text{C}$  for 20 h. After cooling to room temperature, water (20 mL) was added and the precipitate was filtered and washed with water ( $2 \times 20$  mL) and dried in vacuo oven at  $50^{\circ}\text{C}$  for 5 h. The precipitate was treated with Hacac (79.1 mg, 0.7905 mmol) and  $\text{Na}_2\text{CO}_3$  (256.0 mg, 2.37 mmol) in 2-ethoxyethanol (6 mL) at  $100^{\circ}\text{C}$  for 20 h. The product was purified by column chromatography (silica gel,  $\text{CH}_2\text{Cl}_2$ /petroleum ether = 1:1, v/v). A yellow solid was obtained; yield 33.0 mg, 10.0%.  $^1\text{H}$  NMR (400 MHz,  $\text{CDCl}_3$ ):  $\delta$  = 8.87 (d,  $J$  = 5.6 Hz, 1 H), 7.71 (t,  $J$  = 7.2 Hz, 1 H), 7.45 (d,  $J$  = 8.0 Hz, 1 H), 7.25–7.29 (m, 6 H), 7.18–7.22 (m, 4 H), 6.97–7.05 (m, 3 H), 6.75 (d,  $J$  = 8.4 Hz, 1 H), 5.38 (s, 1 H), 1.96 (s, 3 H), 1.72 (s, 3 H) ppm. HRMS (MALDI-TOF): calcd. for  $\text{C}_{28}\text{H}_{25}\text{N}_2\text{O}_2\text{Pt}$   $[\text{M}]^+$  615.1486; found 615.1505.  $\text{C}_{28}\text{H}_{24}\text{N}_2\text{O}_2\text{Pt}$  (616.59): calcd. C 54.63, H 3.93, N 4.55; found C 54.80, H 3.88, N 4.47.

**4-Diphenylamino-4'-(2-pyridyl)biphenyl (L-2)**: 2-(4'-Bromophenyl)pyridine (324.0 mg, 1.38 mmol), triphenyl boronic acid (439.0 mg, 1.52 mmol),  $[\text{Pd}(\text{PPh}_3)_4]$  (80.1 mg, 0.078 mmol), aqueous  $\text{K}_2\text{CO}_3$  (2.76 g, 2.0 M, 10 mL) and toluene (15 mL) were mixed. The mixture was heated at reflux at  $85^{\circ}\text{C}$  for 24 h under Ar. After being cooled, the solvent was evaporated and the organic product was extracted with  $\text{CH}_2\text{Cl}_2$  and dried with  $\text{Na}_2\text{SO}_4$ . The solvent was removed under reduced pressure and the crude product was purified by column chromatography (silica gel, ethyl acetate/hexane = 1:6, v/v). A light-yellow solid was obtained; yield 0.12 g, 19.8%.  $^1\text{H}$  NMR (400 MHz,  $\text{CDCl}_3$ ):  $\delta$  = 8.71 (d,  $J$  = 4.4 Hz, 1 H), 8.05 (d,  $J$  = 8.0 Hz, 2 H), 7.77 (s, 2 H), 7.68 (d,  $J$  = 8.0 Hz, 2 H), 7.53 (d,  $J$  = 8.4 Hz, 2 H), 7.22–7.30 (m, 5 H), 7.14–7.16 (m, 6 H), 7.04 (t,

$J$  = 7.2 Hz, 2 H) ppm. HRMS (EI): calcd. for  $\text{C}_{29}\text{H}_{22}\text{N}_2$   $[\text{M}]^+$  398.1783; found 398.1789.

**Pt-2**: Under Ar, **L-2** (0.11 g, 0.276 mmol) and  $[\text{K}_2\text{PtCl}_4]$  (57.3 mg, 0.138 mmol) were mixed in 2-ethoxyethanol (6 mL) and water (2 mL) and the suspension was heated at  $80^{\circ}\text{C}$  for 20 h. After cooling to room temperature, water (20 mL) was added and the yellow precipitate was washed with water ( $2 \times 20$  mL) and dried in vacuo in an oven. The precipitate was heated in the presence of Hacac (41.4 mg, 0.414 mmol) and  $\text{Na}_2\text{CO}_3$  (131.7 mg, 1.24 mmol) in 2-ethoxyethanol (8 mL) at  $100^{\circ}\text{C}$  for 20 h. Water (10 mL) was added and the yellow precipitate was collected and washed with water ( $2 \times 10$  mL). After drying in vacuo in an oven, the precipitate was purified by column chromatography (silica gel,  $\text{CH}_2\text{Cl}_2$ /petroleum ether = 1:1, v/v). A yellow solid was obtained; yield 15.0 mg, 7.9%.  $^1\text{H}$  NMR (400 MHz,  $\text{CDCl}_3$ ):  $\delta$  = 8.99 (d,  $J$  = 5.6 Hz, 1 H), 7.78–7.83 (m, 2 H), 7.60–7.62 (m, 3 H), 7.47 (d,  $J$  = 8.0 Hz, 1 H), 7.26–7.34 (m, 5 H), 7.14 (d,  $J$  = 7.6 Hz, 6 H), 7.10 (t,  $J$  = 6.0 Hz, 1 H), 7.01 (t,  $J$  = 7.6 Hz, 2 H), 5.48 (s, 1 H), 2.18 (s, 3 H), 2.02 (s, 3 H) ppm.  $^{13}\text{C}$  NMR (100 MHz,  $\text{CDCl}_3$ ):  $\delta$  = 185.96, 184.44, 168.34, 148.02, 147.55, 147.40, 143.61, 141.42, 139.27, 138.24, 135.93, 129.45, 128.58, 128.28, 128.18, 124.665, 124.06, 123.55, 123.06, 122.40, 121.08, 118.51, 102.69, 29.92, 28.46 ppm. HRMS (MALDI-TOF): calcd. for  $\text{C}_{34}\text{H}_{29}\text{N}_2\text{O}_2\text{Pt}$   $[\text{M}]^+$  691.1799; found 691.1816.  $\text{C}_{34}\text{H}_{28}\text{N}_2\text{O}_2\text{Pt} \cdot 0.25\text{CH}_2\text{Cl}_2$  (712.91): calcd. C 57.70, H 4.03, N 3.93; found C 57.76, H 3.94, N 3.77.

**4-Ethynyl-*N,N*-diphenylbenzeneamine (Ethynyl-TPA)**:<sup>[70]</sup> (Trimethylsilyl)acetylene (0.66 mL, 4.64 mmol) and  $\text{CuI}$  (16.0 mg, 0.08 mmol) were added to a degassed solution of 4-bromotriphenylamine (1.0 g, 3.09 mmol),  $[\text{PdCl}_2(\text{PPh}_3)_2]$  (125.6 mg, 0.179 mmol) and  $\text{PPh}_3$  (23.9 mg, 0.091 mmol) in triethylamine (40 mL) and the reaction mixture was heated at reflux for 12 h. Then the mixture was poured into water (50 mL) and extracted with  $\text{CH}_2\text{Cl}_2$  ( $3 \times 50$  mL). The organic layers were dried with  $\text{Na}_2\text{SO}_4$  and the solvents evaporated to dryness. The crude product was purified by column chromatography (silica gel,  $\text{CH}_2\text{Cl}_2$ /petroleum ether = 1:3, v/v). A yellow oil was obtained (the trimethylsilyl protected acetylide); yield 621.8 mg, 58.9%.  $\text{K}_2\text{CO}_3$  (1.00 g, 7.24 mmol) was added to a methanol solution (60 mL) of the yellow oil obtained above (621.8 mg, 1.82 mmol) and the mixture was stirred at room temp. for 24 h. The solvent was evaporated and water (10 mL) was added and then the mixture was extracted with  $\text{CH}_2\text{Cl}_2$ . The organic layer was dried and then the crude product was purified by column chromatography (silica gel,  $\text{CH}_2\text{Cl}_2$ /petroleum ether = 1:3, v/v). A yellow solid was obtained; yield 373.5 mg, 1.01 mmol, 76.2%.  $^1\text{H}$  NMR (400 MHz,  $\text{CDCl}_3$ ):  $\delta$  = 7.32 (d,  $J$  = 8.8 Hz, 2 H), 7.27 (t,  $J$  = 8.4 Hz, 4 H), 7.04–7.11 (m, 6 H), 6.95 (d,  $J$  = 8.4 Hz, 2 H), 3.01 (s, 1 H) ppm. MS (EI): calcd. for  $\text{C}_{20}\text{H}_{15}\text{N}$   $[\text{M}]^+$  269.1204; found 269.1210.

***N*-[4-(2-Pyridyl)phenylethynyl]phenyl-*N,N*-diphenylamine (L-3)**: A solution of ethynyl-TPA (269.0 mg, 1.0 mmol) in THF (10 mL) was added to a degassed solution of 2-(4-bromophenyl)pyridine (234.0 mg, 1.0 mmol),  $[\text{PdCl}_2(\text{PPh}_3)_2]$  (20.6 mg, 0.02 mmol) and  $\text{PPh}_3$  (27.0 mg, 0.1 mmol) in triethylamine (6 mL). Then  $\text{CuI}$  (4.0 mg, 0.02 mmol) was added and the reaction mixture was heated at reflux for 8 h. The mixture was poured into water (20 mL) and extracted with  $\text{CH}_2\text{Cl}_2$  ( $3 \times 30$  mL) and then the combined organic fractions were dried with  $\text{Na}_2\text{SO}_4$  and the solvents evaporated to dryness. The crude product was purified by column chromatography (silica gel, ethyl acetate/hexane = 1:6, v/v). A light-yellow solid was obtained; yield 92.0 mg, 21.8%.  $^1\text{H}$  NMR (400 MHz,  $\text{CDCl}_3$ ):  $\delta$  = 8.70 (d,  $J$  = 4.8 Hz, 1 H), 7.99 (d,  $J$  = 8.4 Hz, 2 H), 7.78–7.75 (m, 4 H), 7.61 (d,  $J$  = 8.4 Hz, 2 H), 7.38

(d,  $J = 8.8$  Hz, 2 H), 7.30–7.24 (m, 3 H), 7.11 (d,  $J = 7.6$  Hz, 4 H), 7.07 (t,  $J = 7.2$  Hz, 2 H), 7.01 (d,  $J = 8.8$  Hz, 2 H) ppm.  $^{13}\text{C}$  NMR (100 MHz,  $\text{CDCl}_3$ ):  $\delta = 156.52, 149.61, 148.01, 147.15, 138.42, 136.97, 132.57, 131.85, 129.40, 126.76, 125.01, 124.33, 123.57, 122.32, 122.22, 120.59, 115.89, 91.11, 88.55$  ppm. HRMS (EI): calcd. for  $\text{C}_{21}\text{H}_{22}\text{N}_2$  [M] $^+$  422.1783; found 422.1790.

**Pt-3:** A mixture of **L-3** (92.0 mg, 0.218 mmol) and  $[\text{K}_2\text{PtCl}_4]$  (45.2 mg, 0.109 mmol) in 2-ethoxyethanol (6 mL) and water (2 mL) was heated at 80 °C for 20 h. After cooling to room temperature, the mixture was added to water (20 mL) and the precipitate was washed with water ( $4 \times 20$  mL) and dried in vacuo in an oven at 50 °C for 5 h. The precipitate was treated with Hacac (0.03 g, 0.30 mmol) in the presence of  $\text{Na}_2\text{CO}_3$  (103.0 mg, 1.00 mmol) in 2-ethoxyethanol (8 mL) at 100 °C for 20 h to give a residue that was purified by column chromatography (silica gel,  $\text{CH}_2\text{Cl}_2$ ). A yellow solid was obtained; yield 12.0 mg, 7.7%.  $^1\text{H}$  NMR (400 MHz,  $\text{CDCl}_3$ ):  $\delta = 9.05$  (d,  $J = 5.6$  Hz, 1 H), 8.17 (s, 1 H), 7.88 (t,  $J = 8.8$  Hz, 1 H), 7.80 (d,  $J = 7.2$  Hz, 2 H), 7.69 (d,  $J = 7.6$  Hz, 2 H), 7.50 (d,  $J = 8.0$  Hz, 1 H), 7.35–7.31 (m, 5 H), 7.21 (t,  $J = 6.8$  Hz, 1 H), 7.17–7.15 (m, 7 H), 6.97 (d,  $J = 8.8$  Hz, 2 H), 5.47 (s, 1 H), 2.01 (s, 3 H), 1.97 (s, 3 H) ppm.  $^{13}\text{C}$  NMR (100 MHz,  $\text{CDCl}_3$ ):  $\delta = 196.40, 193.70, 186.09, 184.72, 167.40, 153.59, 150.83, 147.98, 146.25, 138.56, 132.99, 131.92, 131.69, 129.91, 126.57, 125.75, 125.53, 125.39, 122.90, 119.83, 119.34, 102.72, 29.89, 28.36$  ppm. HRMS (MALDI-TOF): calcd. for  $\text{C}_{36}\text{H}_{28}\text{N}_2\text{O}_4\text{Pt}$  [M] $^+$  747.1697; found 747.1741.  $\text{C}_{36}\text{H}_{28}\text{N}_2\text{O}_4\text{Pt} \cdot 0.25\text{CHCl}_3$  (777.54): calcd. C 56.00, H 3.66, N 3.60; found C 56.16, H 3.60, N 3.53.

**1-(4-Diphenylaminophenyl)-4-(2-pyridylphenyl)ethane-1,2-dione (L-4):** **L-3** (200.4 mg, 0.47 mmol) in 2-ethoxyethanol (6 mL) was heated to 80 °C and  $[\text{K}_2\text{PtCl}_4]$  (83.0 mg, 0.2 mmol) in water (2 mL) was added slowly. Then the reaction mixture was heated at 80 °C for 20 h. After cooling to room temperature the mixture was added to water (20 mL) and the precipitate was washed with water ( $20 \text{ mL} \times 4$ ) and dried in vacuo at 50 °C for 5 h. The precipitate was treated with Hacac (71.0 mg, 0.71 mmol) in the presence of  $\text{Na}_2\text{CO}_3$  (250.0 mg, 2.36 mmol) in 2-ethoxyethanol (6 mL) at 100 °C for 20 h to give a residue that was purified by column chromatography (silica gel, ethyl acetate/hexane = 1:5, v/v). A yellow solid was obtained; yield 30.0 mg, 20.9%.  $^1\text{H}$  NMR (400 MHz,  $\text{CDCl}_3$ ):  $\delta = 8.74$  (d,  $J = 4.8$  Hz, 1 H), 8.15 (d,  $J = 8.4$  Hz, 2 H), 8.10 (d,  $J = 8.8$  Hz, 2 H), 7.78–7.81 (m, 4 H), 7.36–7.29 (m, 5 H), 7.20–7.17 (m, 6 H), 6.98 (d,  $J = 8.8$  Hz, 2 H) ppm.  $^{13}\text{C}$  NMR (100 MHz,  $\text{CDCl}_3$ ):  $\delta = 194.94, 192.65, 155.99, 153.89, 150.19, 146.01, 145.107, 137.13, 133.66, 131.89, 130.56, 129.96, 127.49, 126.68, 125.62, 125.07, 123.33, 121.36, 119.03$  ppm. MS (ESI): calcd. for  $\text{C}_{31}\text{H}_{22}\text{N}_2\text{O}_2$  [M + H] $^+$  455.1760; found 454.1743.

**Luminescent Oxygen Sensing:** A home-assembled flow cell and optical fibre were used for the oxygen sensing. Typical oxygen film preparation is as follows. IMPEK-C polymer (10.0 mg) was dissolved in acetone (0.5 mL) and then the Pt complex in  $\text{CH}_2\text{Cl}_2$  (0.2 mL,  $1.0 \times 10^{-3}$  mol dm $^{-3}$ ) was added to the solution. After thorough mixing, about 0.3 mL of the solution was coated on a silica glass disk (diameter 1.6 cm). The solvent was evaporated at room temp. and a transparent film was obtained. The thickness of the film of **Pt-1** was estimated to be 14.7  $\mu\text{m}$  from the weight of the film (5.1 mg) and the density of the polymer (1.14 g cm $^{-3}$ ). The film thicknesses of the complexes **Pt-2** and **Pt-3** were estimated by the same method to be 11.6 and 14.7  $\mu\text{m}$ , respectively.

**OLED Fabrication and Measurements:** NPB, *m*-MTDATA, CBP and Bphen were obtained commercially and used without further purification. The device configuration is ITO/*m*-MTDATA (30 nm)/NPB(20 nm)/dopant:CBP(30 nm)/Bphen (50 nm)/Al (100 nm) in

which 4,4'-dicarbazolybiphenyl (CBP) served as the host for metal complexes, 4,7-diphenyl-1,10-phenanthroline (Bphen) as the hole blocker and electron-transporting material, 4,4',4''-tris(3-methylphenylphenylamino)triphenylamine (*m*-MTDATA) and 4,4'-bis[(1-naphthyl)phenylamino]biphenyl (NPB) as the hole-injecting and -transporting materials, respectively. Organic layers were deposited by vacuum ( $<1 \times 10^{-3}$  Pa) thermal evaporation on to a clean glass substrate precoated with an indium/tin oxide (ITO) layer with a sheet resistance of ca. 20  $\Omega/\square$ . The 30 nm of *m*-MTDATA, 20 nm of NPB, 30 nm of CBP doped with Pt complex and 50 nm of Bphen were sequentially deposited onto the substrate. Finally, the Al cathode was deposited through a shadow mask by thermal evaporation at  $3 \times 10^{-3}$  Pa in another vacuum chamber. The active area of the device was 9 mm $^2$ . The thicknesses of the organic and metal films were monitored by a quartz crystal microbalance. The current–voltage–brightness (I–V–B) characteristics and spectra of the EL devices were measured with a Keithley 2400 Source meter and a PR-650 Spectra Colorimeter under ambient conditions.

**Supporting Information** (see also the footnote on the first page of this article): Characterization and calculations for compounds.

## Acknowledgments

We thank the National Natural Science Foundation of China (NSFC) (Grants 20642003, 20634040 and 20972024), the Ministry of Education, Scientific Research Foundation for the Returned Overseas Chinese Scholars, the Specialized Research Fund for the Doctoral Program of Higher Education (Grant 200801410004) and the New Century Excellent Talents in University (Grant 08-0077), Changjiang Scholars and Innovative Research Team in University (PCSIRT) (Grant IRT0711), the State Key Laboratory of Fine Chemicals (KF0710 and KF0802), the State Key Laboratory of Chemo/Biosensing and Chemometrics (2008009), the Education Department of Liaoning Province (2009T015) and the Dalian University of Technology (SFDUT07005 and 1000-893394) for financial support. We are grateful to the Royal Society (UK) and NSFC for the China–UK Cost-Share Science Networks.

- [1] J. A. G. Williams, *Top. Curr. Chem.* **2007**, *281*, 205–268.
- [2] G. J. Zhou, Q. Wang, W. Y. Wong, D. Ma, L. X. Wang, Z. Y. Lin, *J. Mater. Chem.* **2009**, *19*, 1872–1883.
- [3] J. Brooks, Y. Babayan, S. Lamansky, P. I. Djurovich, I. Tsyba, R. Bau, M. E. Thompson, *Inorg. Chem.* **2002**, *41*, 3055–3066.
- [4] Z. He, W. Wong, X. Yu, H. Kwok, Z. Lin, *Inorg. Chem.* **2006**, *45*, 10922–10937.
- [5] C. H. Xu, W. Sun, C. Zhang, C. Zhou, C. J. Fang, C. H. Yan, *Chem. Eur. J.* **2009**, *15*, 8717–8721.
- [6] a) T. Lee, C. Chang, Y. Chiu, Y. Chi, T. Chan, Y. Cheng, C. Lai, P. Chou, G. Lee, C. Chien, C. Shu, J. Leonhardt, *Chem. Asian J.* **2009**, *4*, 742–753; b) K. Tsuchiya, S. Yagai, A. Kitamura, T. Karatsu, K. Endo, J. Mizukami, S. Akiyama, M. Yabe, *Eur. J. Inorg. Chem.* **2010**, *6*, 926–933.
- [7] a) A. J. Sandee, C. K. Williams, N. R. Evans, J. E. Davies, C. E. Boothby, A. Köhler, R. H. Friend, A. B. Holmes, *J. Am. Chem. Soc.* **2004**, *126*, 7041–7048; b) K. Tsuchiya, E. Ito, S. Yagai, A. Kitamura, T. Karatsu, *Eur. J. Inorg. Chem.* **2009**, *14*, 2104–2109.
- [8] Z. Yang, J. Feng, A. Ren, *Inorg. Chem.* **2008**, *47*, 10841–10850.
- [9] G. Zhou, Q. Wang, C. Ho, W. Wong, D. Ma, L. Wang, *Chem. Commun.* **2009**, 3574–3576.
- [10] C. Ho, Q. Wang, C. Lam, W. Wong, D. Ma, L. Wang, Z. Gao, C. Chen, K. Cheah, Z. Lin, *Chem. Asian J.* **2009**, *4*, 89–103.

- [11] P. Wu, E. L. Wong, D. Ma, G. S. Tong, K. Ng, C. Che, *Chem. Eur. J.* **2009**, *15*, 3652–3656.
- [12] I. Eryazici, C. N. Moorefield, G. R. Newkome, *Chem. Rev.* **2008**, *108*, 1834–1895.
- [13] I. V. Sazanovich, M. A. H. Alamiry, J. Best, R. D. Bennett, O. V. Bouganov, E. S. Davies, V. P. Grivin, A. J. H. M. Meijer, V. F. Plyusnin, K. L. Ronayne, A. H. Shelton, S. A. Tikhomirov, M. Towrie, J. A. Weinstein, *Inorg. Chem.* **2008**, *47*, 10432–10445.
- [14] a) D. N. Kozhevnikov, V. N. Kozhevnikov, M. M. Ustinova, A. Santoro, D. W. Bruce, B. Koenig, R. Czerwieniec, T. Fischer, M. Zabel, H. Yersin, *Inorg. Chem.* **2009**, *48*, 4179–4189; b) D. Hanss, J. C. Freys, G. Bernardinelli, O. S. Wenger, *Eur. J. Inorg. Chem.* **2009**, *32*, 4850–4859.
- [15] T. J. Wadas, Q. Wang, Y. Kim, C. Flaschenreim, T. N. Blanton, R. Eisenberg, *J. Am. Chem. Soc.* **2004**, *126*, 16841–16849.
- [16] S. C. F. Kui, S. S. Chui, C. Che, N. Zhu, *J. Am. Chem. Soc.* **2006**, *128*, 8297–8309.
- [17] W. Tan, Q. Zhang, J. Zhang, H. Tian, *Org. Lett.* **2009**, *11*, 161–164.
- [18] B. Yin, F. Niemeyer, J. A. G. Williams, J. Jiang, A. Boucekkine, L. Toupet, H. Le Bozec, V. Guerschais, *Inorg. Chem.* **2006**, *45*, 8584–8596.
- [19] G. Zhou, X. Wang, W. Wong, X. Yu, H. Kwok, Z. Lin, *J. Organomet. Chem.* **2007**, *692*, 3461–3473.
- [20] S. Ji, W. Wu, Y. Wu, T. Zhao, F. Zhou, Y. Yang, X. Zhang, X. Liang, W. Wu, L. Chi, Z. Wang, J. Zhao, *Analyst* **2009**, *134*, 958–965.
- [21] J. R. Lakowicz, *Principles of Fluorescence Spectroscopy*, 2nd ed., Kluwer Academic/Plenum Publishers, New York, **1999**.
- [22] a) C. Higgins, D. Wencel, C. S. Burke, B. D. MacCraith, C. McDonagh, *Analyst* **2008**, *133*, 241–247; b) U. Hahn, F. Vögtle, G. De Paoli, M. Staffilani, L. De Cola, *Eur. J. Inorg. Chem.* **2009**, *16*, 2639–2646.
- [23] O. Wolfbeis, R. Narayanaswamy, *Optical sensors: Industrial, Environmental and Diagnostic Applications*, Springer, Berlin, Heidelberg, **2004**.
- [24] C. S. K. Mak, D. Pentlehner, M. Stich, O. S. Wolfbeis, W. K. Chan, H. Yersin, *Chem. Mater.* **2009**, *21*, 2173–2175.
- [25] S. Ji, W. Wu, W. Wu, P. Song, K. Han, Z. Wang, S. Liu, H. Guo, J. Zhao, *J. Mater. Chem.* **2010**, *20*, 1953–1963.
- [26] S. Park, J. E. Kwon, S. H. Kim, J. Seo, K. Chung, S. Park, D. Jang, B. M. Medina, J. Gierschner, S. Y. Park, *J. Am. Chem. Soc.* **2009**, *131*, 14043–14049.
- [27] M. Segal, M. Singh, K. Rivoire, S. Difley, T. V. Voorhis, M. A. Baldo, *Nat. Mater.* **2007**, *6*, 374–378.
- [28] M. Mazzeo, V. Vitale, F. Della Sala, M. Anni, G. Barbarella, L. Favaretto, G. Sotgiu, R. Cingolani, G. Gigli, *Adv. Mater.* **2005**, *17*, 34–39.
- [29] Y. Liu, M. Nishiura, Y. Wang, Z. Hou, *J. Am. Chem. Soc.* **2006**, *128*, 5592–5593.
- [30] P. Coppo, M. Duati, V. N. Kozhevnikov, J. W. Hofstraat, L. De Cola, *Angew. Chem. Int. Ed.* **2005**, *44*, 1806–1810.
- [31] S. J. Lee, C. R. Luman, F. N. Castellano, W. Lin, *Chem. Commun.* **2003**, 2124–2125.
- [32] K. Kalyanasundaram, *Coord. Chem. Rev.* **1982**, *46*, 159–244.
- [33] A. Juris, V. Balzani, F. Barigelletti, S. Campagna, P. Belser, A. V. Zelewsky, *Coord. Chem. Rev.* **1988**, *84*, 85–277.
- [34] C. Wu, B. Bull, K. Christensen, J. McNeill, *Angew. Chem. Int. Ed.* **2009**, *48*, 2741–2745.
- [35] X. Wang, X. Chen, Z. Xie, X. Wang, *Angew. Chem. Int. Ed.* **2008**, *47*, 7450–7453.
- [36] C. Chu, Y. Lo, *Sens. Actuators, B* **2008**, *134*, 711–717.
- [37] G. Zhang, G. M. Palmer, M. W. Dewhirst, C. L. Fraser, *Nat. Mater.* **2009**, *8*, 747–751.
- [38] G. Zhang, J. Chen, S. J. Payne, S. E. Kooi, J. N. Demas, C. L. Fraser, *J. Am. Chem. Soc.* **2007**, *129*, 8942–8943.
- [39] T. Hyakutake, I. Okura, K. Asai, H. Nishide, *J. Mater. Chem.* **2008**, *18*, 917–922.
- [40] M. Niu, H. Fu, Y. Jiang, Y. Zhao, *Synthesis* **2008**, *18*, 2879–2882.
- [41] C. Mousset, A. Giraud, O. Provot, A. Hamze, J. Bignon, J. Liu, S. Thoret, J. Dubois, J. Brion, M. Alami, *Bioorg. Med. Chem. Lett.* **2008**, *18*, 3266–3271.
- [42] C. Che, C. Kwok, S. Lai, A. F. Rausch, W. J. Finkenzeller, N. Zhu, H. Yersin, *Chem. Eur. J.* **2010**, *16*, 233–247.
- [43] S. Ji, J. Yang, Q. Yang, S. Liu, M. Chen, J. Zhao, *J. Org. Chem.* **2009**, *74*, 4855–4865.
- [44] J. Hu, J. H. K. Yip, D. Ma, K. Wong, W. Chung, *Organometallics* **2009**, *28*, 51–59.
- [45] Y. Chen, S. Li, Y. Chi, Y. Cheng, S. Pu, Y. Yeh, P. Chou, *ChemPhysChem* **2005**, *6*, 2012–2017.
- [46] a) Y. Liu, J. Feng, A. Ren, *J. Phys. Chem. A* **2008**, *112*, 3157–3164; b) T. Ruiu, C. Garino, L. Salassa, A. M. Pizarro, C. Nervi, R. Gobetto, P. J. Sadler, *Eur. J. Inorg. Chem.* **2010**, *8*, 1186–1195.
- [47] A. Vlček Jr., S. Zališ, *Coord. Chem. Rev.* **2007**, *251*, 258–287.
- [48] O. A. Borg, S. S. M. C. Godinho, M. J. Lundqvist, S. Lunell, P. Persson, *J. Phys. Chem. A* **2008**, *112*, 4470–4476.
- [49] G. Zhao, J. Liu, L. Zhou, K. Han, *J. Phys. Chem. B* **2007**, *111*, 8940–8945.
- [50] F. Han, L. Chi, X. Liang, S. Ji, S. Liu, F. Zhou, Y. Wu, K. Han, J. Zhao, T. D. James, *J. Org. Chem.* **2009**, *74*, 1333–1336.
- [51] Z. Yang, J. Feng, A. Ren, *Inorg. Chem.* **2008**, *47*, 10841–10850.
- [52] a) X. Liu, J. Feng, J. Meng, Q. Pan, A. Ren, X. Zhou, H. Zhang, *Eur. J. Inorg. Chem.* **2005**, 1856–1866; b) M. Osawa, I. Kawata, S. Igawa, A. Tsuboyama, D. Hashizume, M. Hoshino, *Eur. J. Inorg. Chem.* **2009**, *25*, 3708–3711.
- [53] B. Valeur, *Molecular Fluorescence: Principles and Applications*, Wiley-VCH, **2001**.
- [54] C. L. Yang, X. W. Zhang, H. You, L. Y. Zhu, L. Q. Chen, L. N. Zhu, Y. T. Tao, D. G. Ma, Z. G. Shuai, J. G. Qin, *Adv. Funct. Mater.* **2007**, *17*, 651–661.
- [55] R. P. Briñas, T. Troxler, R. M. Hochstrasser, S. A. Vinogradov, *J. Am. Chem. Soc.* **2005**, *127*, 11851–11862.
- [56] D. B. Papkovsky, T. C. O’Riordan, *J. Fluoresc.* **2005**, *15*, 569–584.
- [57] L. H. Fischer, M. I. J. Stich, O. S. Wolfbeis, N. Tian, E. Holder, M. Schäferling, *Chem. Eur. J.* **2009**, *15*, 10857–10863.
- [58] H. Guo, S. Ji, W. Wu, W. Wu, J. Shao, J. Zhao, *Analyst*, DOI:10.1039/C0AN00404A.
- [59] Z. Wang, T. Chen, J. Xu, *Macromolecules* **2000**, *33*, 5672–5679.
- [60] N. Leventis, A. M. M. Rawashdeh, I. A. Elder, J. Yang, A. Dass, C. Sotiropoulos, *Chem. Mater.* **2004**, *16*, 1493–1506.
- [61] H. Zhang, Y. Sun, K. Ye, P. Zhang, Y. Wang, *J. Mater. Chem.* **2005**, *15*, 3181–3186.
- [62] B. Wang, Y. Liu, B. Li, S. Yue, W. Li, *J. Lumin.* **2008**, *128*, 341–347.
- [63] T. S. Yeh, C. S. Chu, Y. L. Lo, *Sens. Actuators, B* **2006**, *119*, 701–707.
- [64] B. J. Basu, *Sens. Actuators, B* **2007**, *123*, 568–577.
- [65] M. J. Frisch, G. W. Trucks, H. B. Schlegel, G. E. Scuseria, M. A. Robb, J. R. Cheeseman, G. Scalmani, V. Barone, B. Mennucci, G. A. Petersson, H. Nakatsuji, M. Caricato, X. Li, H. P. Hratchian, A. F. Izmaylov, J. Bloino, G. Zheng, J. L. Sonnenberg, M. Hada, M. Ehara, K. Toyota, R. Fukuda, J. Hasegawa, M. Ishida, T. Nakajima, Y. Honda, O. Kitao, H. Nakai, T. Vreven, J. A. Montgomery Jr., J. E. Peralta, F. Ogliaro, M. Bearpark, J. J. Heyd, E. Brothers, K. N. Kudin, V. N. Staroverov, R. Kobayashi, J. Normand, K. Raghavachari, A. Rendell, J. C. Burant, S. S. Iyengar, J. Tomasi, M. Cossi, N. Rega, J. M. Millam, M. Klene, J. E. Knox, J. B. Cross, V. Bakken, C. Adamo, J. Jaramillo, R. Gomperts, R. E. Stratmann, O. Yazyev, A. J. Austin, R. Cammi, C. Pomelli, J. W. Ochterski, R. L. Martin, K. Morokuma, V. G. Zakrzewski, G. A. Voth, P. Salvador, J. J. Dannenberg, S. Dapprich, A. D. Daniels, Ö. Farkas, J. B. Foresman, J. V. Ortiz, J. Cioslowski, D. J. Fox, *Gaussian 09*, Revision A.1, Gaussian, Inc., Wallingford, CT, **2009**.
- [66] G. M. Sheldrick, *Acta Cryst.* **2008**, *A64*, 112–122.

- [67] H. Xiao, H. Shen, Y. Lin, J. Su, H. Tian, *Dyes Pigm.* **2007**, *73*, 224–229.
- [68] Z. H. Li, M. S. Wong, *Org. Lett.* **2006**, *8*, 1499–1502.
- [69] G. Zhou, W. Wong, B. Yao, Z. Xie, L. Wang, *Angew. Chem. Int. Ed.* **2007**, *46*, 1149–1151.
- [70] K. Onitsuka, N. Ohara, F. Takei, S. Takahashi, *Dalton Trans.* **2006**, 3693–3698.

Received: March 24, 2010  
Published Online: August 24, 2010